PHYSICAL REVIEW E **70**, 055402(R) (2004)

Fast electron heating of a solid target in ultrahigh-intensity laser pulse interaction

E. Martinolli,[1] M. Koenig,[1] F. Amiranoff,[1] S. D. Baton,[1] L. Gremillet,[3] J. J. Santos,[1] T. A. Hall,[2] M. Rabec-Le-Gloahec,[3] C. Rousseaux,[3] and D. Batani[4]

[1]*Laboratoire pour l'Utilisation des Lasers Intenses, UMR7605, CNRS-CEA-Université Paris VI-Ecole Polytechnique, 91128 Palaiseau, France*

[2]*University of Essex, Colchester CO4 3SQ, United Kingdom*

[3]*Commissariat à l'Energie Atomique, DIF-BP1, 91680 Bruyères-le-Châtel, France*

[4]*Dipartimento di Fisica G. Occhialini, Università di Milano-Bicocca-INFM, 20126 Milan, Italy*

(Received 20 October 2003; revised manuscript received 1 March 2004; published 22 November 2004)

We report one of the first measurements of induced heating due to the transport of a fast electron beam generated by an ultrashort pulse laser interaction with solid targets. Rear-side optical reflectivity and emissivity have been used as diagnostics for the size and temperature of the heated zone. A narrow spot has been observed of the order of the laser focus size. Values up to ~10 eV at the target back surface were inferred from the experimental data and compared with the predictions of a hybrid collisional-electromagnetic transport simulation.

DOI: 10.1103/PhysRevE.70.055402 PACS number(s): 52.50.Jm, 52.38.Kd, 52.57.Kk

In the fast ignition [1] approach to inertial confinement fusion (ICF), a few kJ of relativistic suprathermal electrons produced by an ultraintense laser pulse should deposit their energy in the dense fuel in a small area (≈ 10 μm size) and heat it to a high temperature (≈ 10 keV), enough to ignite thermonuclear reactions [2]. Therefore, one of the key issues is to study the energy transport in dense matter by laser-accelerated fast electrons (FE) and to determine the temperature and geometry of the heated zone. Important results have been already obtained: it has been shown [3–5] how electron propagation is strongly influenced by self-generated electric fields, as predicted theoretically [6]. A very few experiments have been performed regarding a quantitative measurement of the heating induced in the target by FE [7–9]. The occurrence of collimated propagation of fast electrons has been shown [10–13], but the relevance to fast ignition is doubtful since it is not clear what energy is effectively involved in the "relativistic FE jets." The diagnostic used in those experiments [10–12] is sensitive to changes in the ionization of the target, which could be induced by a *small number* of FE. It is therefore much more important to detect a localized heating which would directly prove the transport of the FE bulk population. The heating is strongly coupled to the propagation geometry: a more collimated beam implies higher temperatures [13]. In this paper we present one of the first experiments providing a quantitative measurement of target heating based on optical diagnostics. In order to detect the perturbation due to FE energy deposition, we used space and time-resolved measurements of rear surface reflectivity and self-emission, previously used in laser shock experiments [14,15]. We also used the so-called chirped pulse reflectivity technique [16] (CPR) in order to obtain a ps time resolution over a 100 ps time interval. The experiment was performed at the LULI Laboratory on the 100 TW laser. A 350 fs, 1.057 μm 10 J laser pulse was focused by an $f/3$ off-axis parabola at normal incidence onto flat Al targets with thickness ranging from 20 to 100 μm. The laser focal spot was ≈ 20 μm full width at half maximum corresponding to a maximum incident laser intensity of $\approx 10^{19}$ W cm^{-2}. The ASE contrast ratio was $\sim 10^{-7}$, giving an intensity of $(2-3)\times 10^{12}$ W cm^{-2} over 2 ns. Thanks to four Pockels cells, no significant prepulse was present.

The rear surface reflectivity was measured with a $\lambda = 0.528$ μm *p*-polarized 350 fs probe beam (Fig. 1). Specular reflection (45°) of the probe on the target was image-relayed onto a visible CCD camera with a 10 μm spatial resolution. Two-dimensional (2D) snapshots of the target were obtained at different times (0–40 ps) after the interaction, by varying the probe beam delay line (time precision ≈ 5 ps). Before each shot, cold target reflectivity was measured as a reference. In order to better study the target heating dynamics, for some shots the probe beam was only partially time-compressed to 50 ps and used to obtain 1D time-resolved images, with 2–3 ps time resolution over a 100 ps window, by means of the chirped pulse technique. The reflected probe beam was sent to the entrance slit of a visible imaging spectrometer coupled to a CCD camera, obtaining spatial resolution on the slit axis and time resolution by the probe chirp on the other axis. Visible self-emission (350–800 nm) was also used as a diagnostic for temperature and heating dynamics: the target rear surface was image-relayed at 0 degrees onto

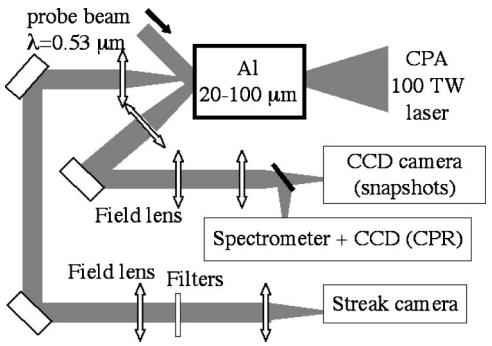

FIG. 1. Experimental setup (optical reflectivity and self-emission diagnostics).

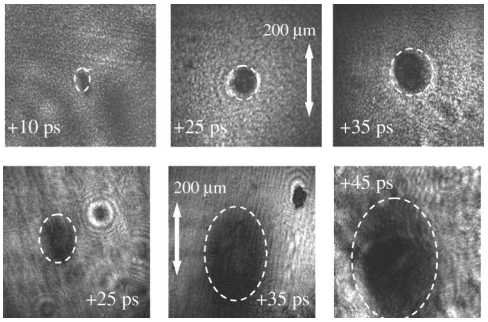

FIG. 2. Snapshots of aluminum target rear side reflectivity (45°) obtained with a 350 fs probe beam. Main beam irradiance was a few 10^{18} W cm^{-2}. Target thickness: 20 μm (top), 75 μm (bottom).

the entrance slit of a streak camera (Fig. 1), with a 10 ns time window and less than 100 ps time resolution. Filters stopped spurious 2ω light from the front plasma and the scattering of the probe beam from the rear surface. The imaging system transmission and the streak camera response were absolutely calibrated with a spectral lamp and a ns probe laser, respectively.

The two snapshot sequences (Fig. 2) show a dark, low reflectivity spot, which expands at an average radial speed of $(2-3)\times10^6$ m/s. At the center, reflectivity drops to values below 0.3. For thin targets (20 μm), the spot diameter increases from 30 to 150 μm during the first 35 ps after the main pulse. At the earliest time (10 ps), the spot size is only slightly larger than the laser focal spot, which suggests some beaming of the FE current. For thicker targets (75 μm), the spot is bigger at the same time delay and has less sharp contours. Chirped pulse data (Fig. 3) allow us to observe more in detail dynamics of the spot. Reflectivity starts to decrease after the main pulse interaction ($t=0$) and drops to a minimum in 5–10 ps. At the same time, the spot expands with a high initial radial velocity $\approx(8-9)\times10^6$ m/s, decreasing to $\approx10^6$ m/s after 30 ps (Fig. 3, bottom). The time-averaged value of the expansion velocity is consistent with that estimated from snapshot sequences.

A low reflectivity indicates heating of the rear surface, which we relate to FE energy deposition. This occurs on the FE transit time scale ($\sim$1 ps), i.e., instantaneously compared to our time resolution. Other processes, which may contribute to heating, do not play a significant role here: prompt x-ray preheating (from front side plasma) would be too weak and spatially spread, while ASE shock preheating can be discarded, as we will show in detail. The electron-deposited energy heats the rear surface above the aluminum vaporization temperature, thus creating a plasma which expands to vacuum and cools down on a ns time scale. For a steplike gradient, the reflectivity dependence versus temperature shows a broad minimum between 1 and 100 eV, using Drude's model and Lee and More's electron-ion collision frequency [17] to link reflectivity to conductivity. Experimental reflectivity values at spot center (5–30%) correspond to such a range of temperatures. However, on our ps time scale, the steplike approximation no longer holds, due to hydrodynamic expansion. This was therefore calculated using MULTI hydrodynamic code [18], for different *initial* electron temperatures of the target. At each time step during expansion, we calculated the reflectivity by solving Helmholtz's equation [19] for the incident and reflected probe beam through the density gradient given by the code (multilayer dielectric approximation [15,20]). In Fig. 4, we compare the experimental points with simulated reflectivity curves. Snapshots data are consistent with a broad temperature range (from a few eV up to $\approx$100 eV).

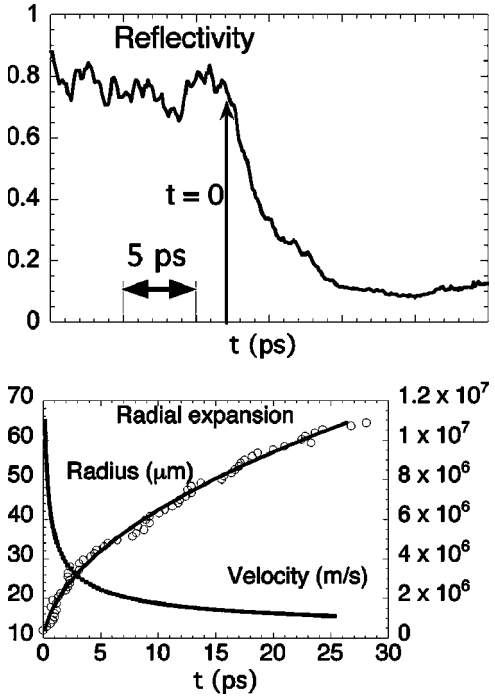

FIG. 3. Chirped pulse reflectivity on a 25 μm aluminum target. Reflectivity (top) drops to low values after the interaction time, while the spot expands radially (bottom).

For what concerns the radial expansion of the heated spot, the observed high velocity 1000 km/s cannot be due to any shock-driven hydrodynamic expansion, which typical velocity is $\leqslant$10 km/s. Moreover, a radial conduction wave or a blast wave model cannot reproduce the observed velocities assuming a realistic energy source. Such a fast expansion rather suggests other processes, related to FE transport dynamics, which are not completely understood so far and are

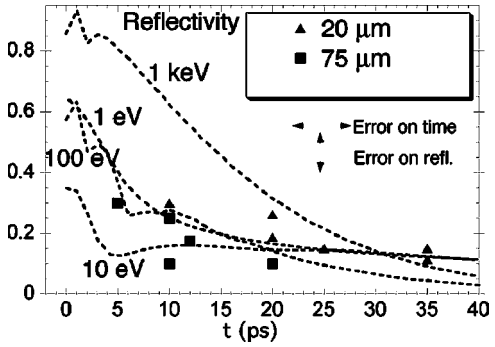

FIG. 4. Comparison between reflectivity data points vs time (snapshots) and simulations (dotted curves) for different initial target temperatures.

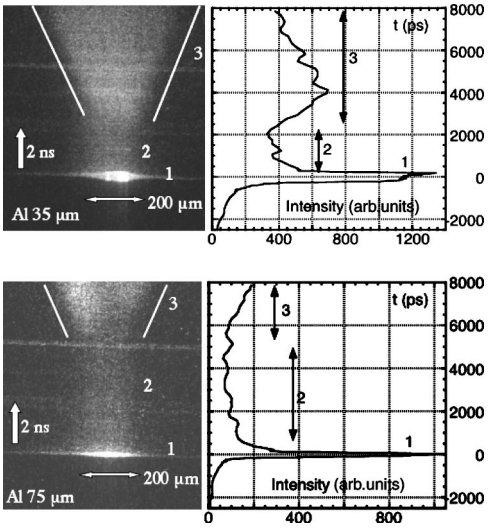

FIG. 5. Time-resolved rear side optical self-emission for 35 and 75 μm Al targets. Vertical cross sections at spot center show a three-phase time structure.

currently under investigation both from the theoretical and the experimental point of view. (a) An effect related to the FE "sheath potential" at target rear side ("fountain" effect). This sheath [21] traps the electrons which, in principle, could reflux and quickly heat the surrounding cold target, thus lowering the reflectivity. (b) FE propagate through the target as a cloud [10]: the fastest, traveling on the laser axis, reach the rear surface before the slower lateral ones, producing an "apparent" expansion of the spot. The modeling of such a process is beyond the scope of this paper. To refine the temperature measurement, we shall discuss the self-emission data (Fig. 5). These show a three-phase time structure, which is reproducible of shot to shot, independently of the target thickness. (1) A short ($<$50 ps), bright prompt signal. This peak is related to the arrival of FE at target rear side. This signal can be explained in terms of optical transition radiation (OTR) and synchrotron radiation (SR) [22]. (2) After the peak, a *decreasing emissivity*, which we relate to thermal (blackbody) emission following the rapid heating of the material by FE. We detect the cooling/expansion phase of the relatively hot plasma created at the target rear side. The spot size of self-emission (100–150 μm) corresponds to the reflectivity spot size at the end of the rapid expansion previously described, showing that both diagnostics are consistent. (3) At later times, a few ns after the bright peak depending on target thickness, emission intensity increases again and lateral expansion is observed. This process, slower than FE energy release, corresponds to the ASE shock breakout. The time delay between the first bright peak and this breakout is approximately 2 ns for 35 μm and 6 ns for 75 μm targets. It increases with thickness giving a velocity of $\sim$10 km/s, which corresponds to LULI laser ASE shock speed. According to detailed hydrodynamic simulations at maximum ASE level (5×10^{12} W cm^{-2} over 2 ns), the shock always reaches the rear surface well *after* the interaction, in full agreement with emissivity data. At initial times, the emissivity is directly related to the brightness temperature of the surface, but it is masked by the huge OTR peak (1). We

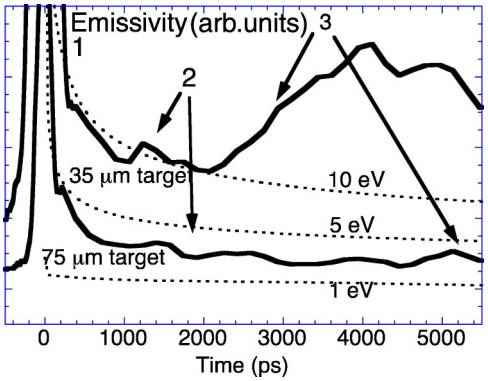

FIG. 6. Comparison between experimental self-emission vs time and simulations (dotted curves) for different initial target temperatures.

therefore studied self-emission *after* the peak (phase 2). We calculated the emissivity from the expanding plasma given by hydrodynamic simulations, accounting for the absorption, as in shock temperature measurements [14]. In Fig. 6, we compare the emission calculated for different *initial* temperatures (dotted lines) with the experimental profile (solid line) taken at the center of the spot. We note that the fluctuation of the emissivity value is not a significant feature. In the cooling phase (2), results are consistent with an initial temperature of $\approx$10 eV for 35 μm targets and 2–3 eV for thicker 75 μm targets, in agreement with reflectivity data.

We compared our experimental results with the predictions of the PARIS [23] transport code, for conditions close to the experimental ones. We assumed a 1D Maxwellian FE source related to the laser irradiance through Beg's scaling law [24], a 15% laser-to-FE energy conversion [5], and a 20

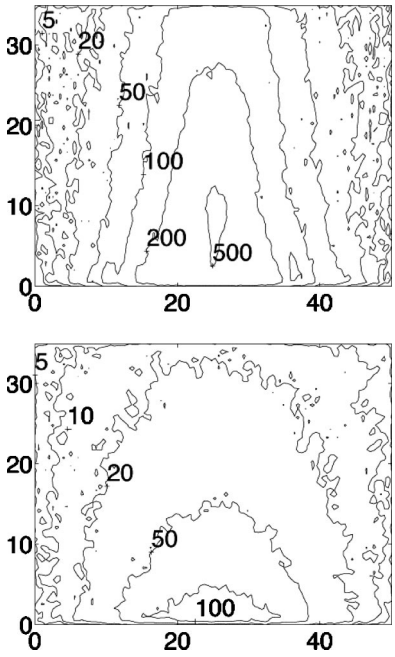

FIG. 7. 2D plot of simulated target temperature (eV) 1.7 ps after the CPA pulse, with (top) and without (bottom) self-generated **E** and **B** fields. Size in μm.

degrees initial angular spread [7,22]. The simulation corresponds to the initial situation we can detect on our reflectivity diagnostic: Fig. 7 shows the spatial temperature distribution 1.7 ps after the laser interaction, with or without the self-generated **E** and **B** fields. A purely collisional propagation reproduces quite well the observed temperature and the initial heated spot size, whereas in the presence of the fields the temperature seems to be overestimated (additional energy is deposited by the return current). Heating is calculated using an equation of state (EOS) [25], and the Lee and More model [17] is used for ionization and conductivity, both supposing thermodynamic equilibrium and a single temperature. The validity of this approach at the short time scale considered is an open question.

In conclusion, in this paper we have reported a quantitative measurement of target heating induced by the propagation of FE in solid density targets using optical diagnostics (time-resolved reflectivity and emissivity). In our conditions, the target is heated up to $\sim$10 eV after the breakout of the FE front. A radial expansion of the rear side heated spot ($30-150$ μm) has been detected with a 2 ps time resolution, giving a high radial velocity (a few 10^6 m/s) decreasing with time. These results provide quantitative data on the geometry and dynamics of the rear surface heating by FE energy transport. However, in order to better understand the complex phenomena taking place at the rear side (potential sheath, refluxing, ion acceleration, hydrodynamic expansion), a more direct measurement of target perturbation will be needed, i.e., time-dependent x-ray absorption/emission (FE current and heating) and proton radiography (hydrodynamic expansion and electric fields). Moreover, a more realistic description of the FE breakout and energy relaxation needs to be folded into FE transport codes to reproduce the observed temperature level.

This work was supported by EU TMR Laser Facility Access Program (ERBFMGE-CT95-0044), E1127 Ile-de-France Reg. Grant, and the ESF FEMTO program.

[1] M. Tabak *et al.*, Phys. Plasmas **1**, 1626 (1994).
[2] S. Atzeni, in *Matter in Super-intense Laser Fields*, edited by C. Joachain and D. Batani (Plenum, New York, 2000).
[3] T. Hall *et al.*, Phys. Rev. Lett. **81**, 1003 (1998).
[4] D. Batani *et al.*, Phys. Rev. E **61**, 5725 (2000).
[5] F. Pisani *et al.*, Phys. Rev. E **62**, R5927 (2000).
[6] A. R. Bell *et al.*, Phys. Rev. E **58**, 2471 (1998).
[7] M. H. Key *et al.* in IFSA 2001, Kyoto, Japan (2001).
[8] M. Zepf *et al.*, in *4th Workshop on Fast Ignition of Fusion Targets* (LULI Ecole Polytechnique, Palaiscau, 2000).
[9] K. A. Tanaka *et al.*, Phys. Plasmas **7**, 2014 (2000).
[10] L. Gremillet *et al.*, Phys. Rev. Lett. **83**, 5015 (1999).
[11] M. Borghesi *et al.*, Phys. Rev. Lett. **83**, 4309 (1999).
[12] M. Tatarakis *et al.*, Phys. Rev. Lett. **81**, 999 (1998).
[13] J. A. Koch *et al.*, Phys. Rev. E **65**, 016410 (2001).
[14] T. Hall *et al.*, Phys. Rev. E **55**, R6356 (1997).
[15] A. Benuzzi *et al.*, Phys. Plasmas **5**, 1 (1998).
[16] A. Benuzzi-Mounaix *et al.*, Phys. Rev. E **60**, R2488 (1999).
[17] Y. T. Lee and R. M. More, Phys. Fluids **27**, 273 (1984).
[18] R. Ramis *et al.*, Comput. Phys. Commun. **49**, 475 (1988).
[19] P. Celliers and A. Ng, Phys. Rev. E **47**, 3547 (1993).
[20] M. Basko *et al.*, Phys. Rev. E **56**, 1019 (1997).
[21] S. C. Wilks *et al.*, Phys. Plasmas **8**, 542 (2001).
[22] J. J. Santos *et al.*, Phys. Rev. Lett. **89**, 025001 (2002).
[23] L. Gremillet *et al.*, Phys. Plasmas **9**, 941 (2002).
[24] F. N. Beg *et al.*, Phys. Plasmas **4**, 447 (1997).
[25] SESAME: The LANL EOS database, LA-UR-92-3407, LANL (1992).